IOP Conf. Series: Materials Science and Engineering **219** (2017) 012018 doi:10.1088/1757-899X/219/1/012018

Electron tomography of dislocations in an Al-Cu-Mg alloy

Z.Q. Feng [1,2], C.W. Lin [1], T.T. Li [1], X. Luo [1], G.L. Wu [1], X.X. Huang [1]
[1] College of Materials Science and Engineering, Chongqing University, Chongqing 400044, China
[2] Electron Microscopy Center of Chongqing University, Chongqing University，Chongqing 400044, China

E-mail: zqfeng@cqu.edu.cn

Abstract. Dislocation loops and helices are typical dislocation structures in quenched Al-Cu-Mg alloys. In this study, we combine electron tomography and Burgers vector analysis to characterize the spatial arrangement and crystallographic features of such dislocation loops and helices. It is found that the dislocation loops are fully edge in character and on {011} planes. The axis of each dislocation helix formed during quenching is found to be parallel to the Burgers vectors of the helix, which is always of <011> type.

1. Introduction

Dislocation loops and helices are two typical types of intrinsic dislocations generated during water quenching from the solid solution treatment temperature in precipitation-hardenable Al alloys [1]. The presence of these dislocations and their morphological and crystallographic characteristics will affect the aging behaviour of the alloys. Previous investigations have indicated that dislocation loops formed during quenching are usually full dislocations of mixed edge and screw character on {111} planes, and that they can form through the reaction of a moving Shockley partial dislocation (a/6<112>) with Frank partial dislocation loops (a/3<111>), formed by the condensation and collapse of quenched-in vacancies on the close-packed {111} planes [2]. However, in a study of the dislocation sources in a quenched Al-7%Mg alloy, Embury et al. [3] observed that the condensation and collapse of quenched-in vacancies actually occurred on $\{011\}_{Al}$ planes, and that the resultant dislocation loops possessed an a/2<110> type Burgers vector. Moreover, recent transmission electron microscopy (TEM) investigations of a quenched Al-Cu-Mg alloy revealed that all the dislocation loops are of pure edge character and lie on {011} planes [4]. As to the helical dislocations, they can form via the reaction of prismatic dislocation loops with straight screw dislocation lines, or the through climb of a mixed dislocation segment with its ends pinned by solute atoms or some other obstacles [2,5]. The Burgers vector of a helical dislocation is always parallel to its helical axis [2,6]. The helical axis was often observed to be approximately parallel to the <011> direction, but a <001> helix axis direction has also been reported [5,7-9]. These different observations of the crystallographic characteristics of dislocation loops and helices could be caused by the two-dimensional (2D) analysis of the crystallographic and morphological features of the dislocation loops and helices. A more precise characterization is thus required to fully understand the nature of such dislocation loops and helices.

Dislocation electron tomography has been developed and applied to study the three-dimensional (3D) morphology of dislocation structures [10,11] and to visualize the details of the interaction of moving dislocations with grain boundaries and precipitate particles [12]. In this study, we combine

electron tomography and Burgers vector analysis to characterize the 3D configuration and crystallography of dislocation helices and loops in a quenched Al-Cu-Mg alloy.

2. Experimental

A commercial AA2024 aluminum alloy sheet with the nominal composition of Al-4.2Cu-1.5Mg-0.6Mn-0.5Fe-0.5Si (wt%) was chosen for this study. Several small specimens were cut and solid solution-treated at 495 ℃ for 1 h, followed by water quenching. To prepare thin foil samples for TEM observations, the treated specimens were mechanically ground and punched into disks of 3 mm in diameter. The small disks were finally thinned by twin-jet electropolishing with a solution of 30% nitric acid and 70% methanol at a temperature below -25 ℃ at 15V.

TEM observations were performed using a 200kV Tecnai 20 electron microscope equipped with a fully automated TEM tomography system. A single tilt tomography holder (Fischione model 2020) was used to acquire several tilt series of dark field (DF) images over a tilt angle range from -70° to +70° with an increment of 1°. A precision sample mounting system developed in house was used to control the diffraction contrast conditions during the entire tilting process for data acquisition. The tomography data were aligned and reconstructed using the Inspect 3D software, and finally visualized in 3D using the Avizo 9.0 software. All the dislocations, irrespective of their 3D morphology, were recognized as full dislocations, and their Burgers vectors were determined according to the invisibility criterion ($\boldsymbol{g}\cdot\boldsymbol{b} = 0$) for full dislocations in typical face centered cubic (FCC) crystals.

3. Results and discussion

Figure 1 shows two examples of 2D projections of the dislocation structure observed in the quenched Al-Cu-Mg alloy. A high density of dislocations, especially dislocation helices and loops (figure 1b), are observed within the Al grain matrix. Note that some of the dislocations overlap with each other in these 2D images, leaving an open question as to whether or not they are actually in contact and interacting, or if they are spatially separated. To characterize the crystallographic features and spatial arrangements of these dislocations, detailed TEM crystallographic analysis, as well as electron tomography, was carried out. For the dislocations in the area of interest as shown in figure 1b, five reflections, namely $\boldsymbol{g}$=[020], [00$\bar{2}$], [0$\bar{2}\bar{2}$], [1$\bar{1}$1]and [$\bar{1}\bar{1}\bar{1}$] that are related to the two crystal zone axes of [1$\bar{1}$0] and [100] were chosen to obtain DF images of the dislocations (figure 2). Based on the dislocation invisibility criterion, the Burgers vectors for all dislocations seen in this area (figure 1b) were fully determined (see table 1).

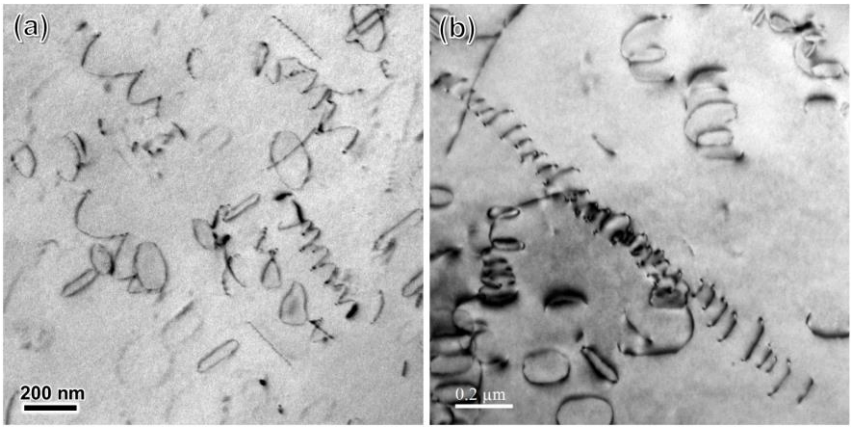

Figure 1. TEM images showing typical observations of dislocation helices and loops in an Al-Cu-Mg alloy after solid solution treatment and water quenching. A detailed analysis of dislocation Burgers vectors and tomography was carried out for the dislocations shown in (b) (for details see figure 2 and figure 3).

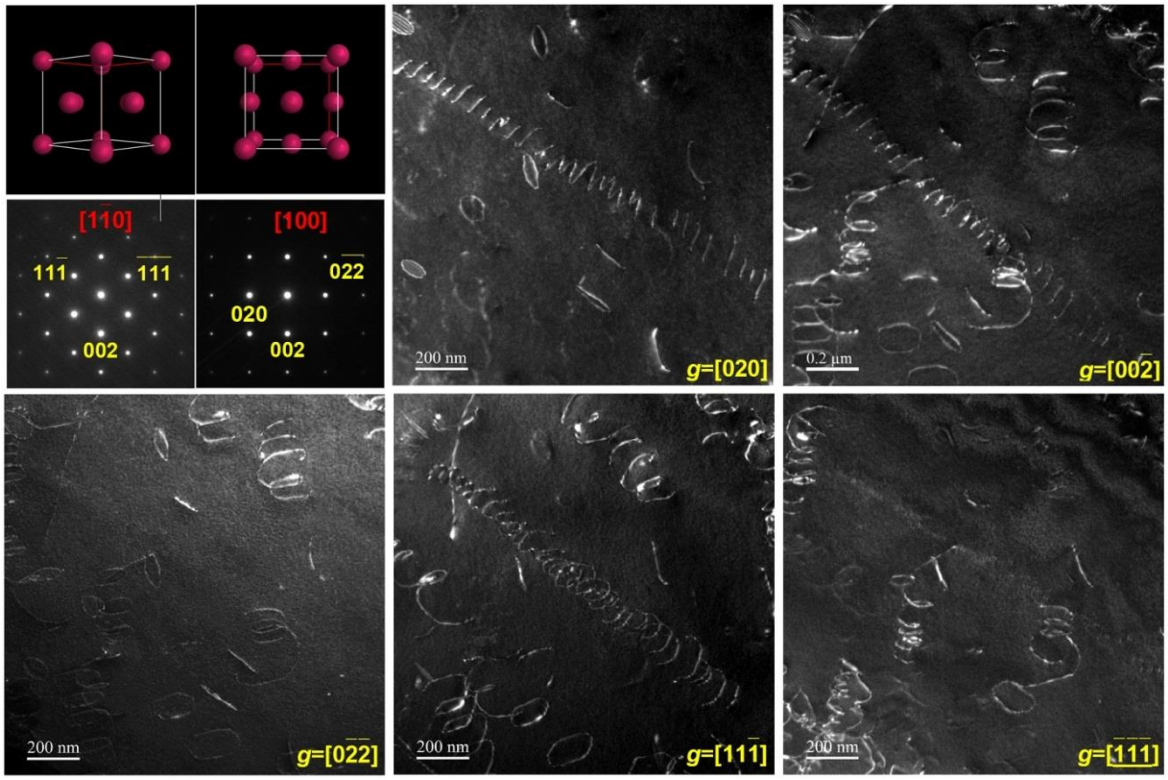

Figure 2. Top-left: [1$\bar{1}$0] and [100] oriented FCC crystal units and corresponding diffraction patterns with self-consistent indexing; Rest: DF images using different reflections ***g***=[020], [00$\bar{2}$], [0$\bar{2}\bar{2}$], [11$\bar{1}$] and [$\bar{1}\bar{1}\bar{1}$] as labelled in the figures.

Table 1. Visibility analysis of possible full dislocations in FCC crystals for five selected reflection vectors ***g*** (★ indicates that the dislocation is visible).

b / ***g***	***b*** (×a/2)					
	[110]	[1$\bar{1}$0]	[101]	[10$\bar{1}$]	[011]	[01$\bar{1}$]
[020]	★	★			★	★
[00$\bar{2}$]			★	★	★	★
[0$\bar{2}\bar{2}$]	★	★	★	★	★	
[11$\bar{1}$]	★			★		★
[$\bar{1}\bar{1}\bar{1}$]	★		★		★	

To understand the dislocation morphology and configuration in 3D, DF-TEM electron tomography was employed. With the aid of a precision sample mounting system, a constant two-beam condition (***g*** = [002]) was well controlled during a single tilt data acquisition process. A tilt series of DF dislocation images as well as corresponding diffraction patterns from -70° to +70° were then obtained and are shown in Figure 3, together with the corresponding unit cell geometry. It can be seen that the diffraction contrast conditions for dislocations during the image acquisition process were rather stable, and most of the images including the ones taken at high tilt angles are in good contrast. A few images taken when the beam directions were close to zone axes are of poor contrast; such images were not

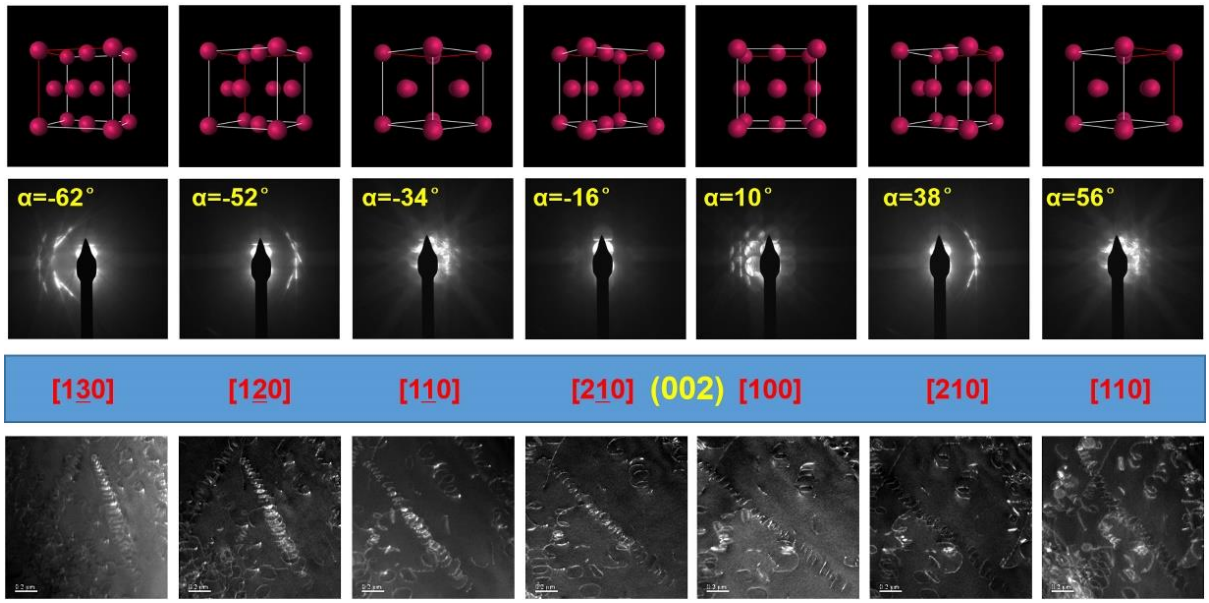

Figure 3. The typical crystal orientations and corresponding diffraction patterns and DF images in the tilt series from -70° to 70° by using reflection $\boldsymbol{g}$=[002].

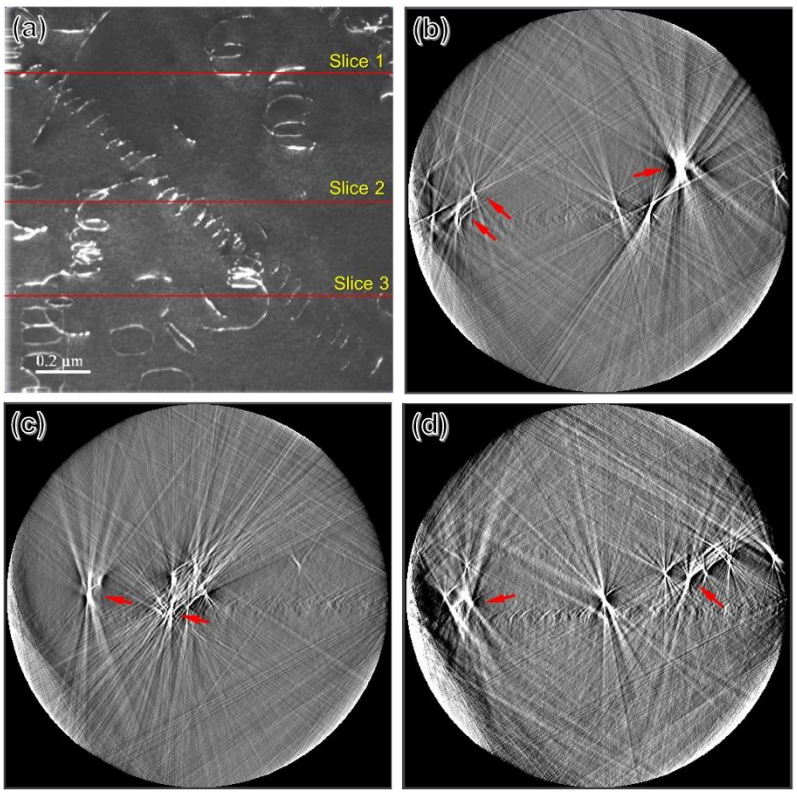

Figure 4. (a) DF image at zero tilt; (b-d) the back-projected cross-sections corresponding to slices 1-3 in (a) showing the quality of tilt axis alignment.

used for the 3D reconstruction. Image alignment using cross correlation algorithm [13-15] exhibited good quality of position and tilt axis alignment, which can be seen more clearly in three back-projected cross-sections as shown in figure 4. In particularly, it can be noted that the projections of

some dislocations show circular-arc cross-sections (see arrows), and some of them are too close to be clearly distinguished, which may affect the resolution in the projection direction.

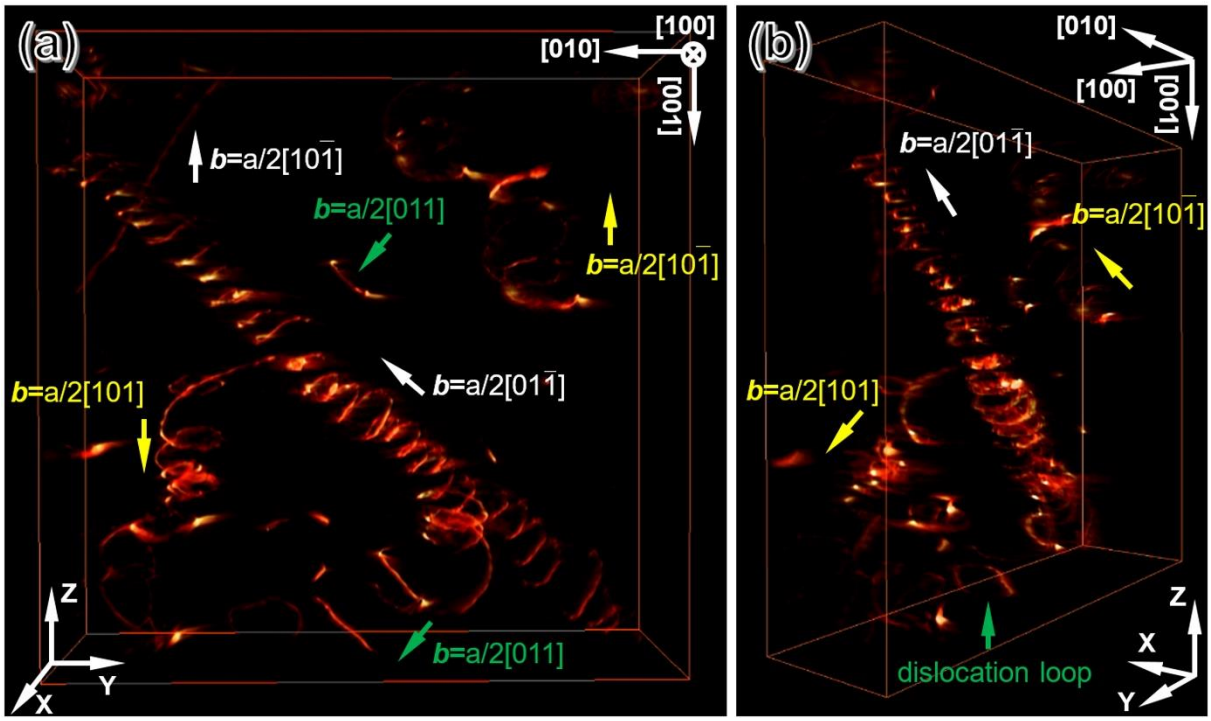

Figure 5. Two projections of 3D reconstruction of the dislocation structure in Figure 2b. Note that (a) is tilted 10° to transform from original sample coordinate system to the crystal coordinate system.

The weighted back projection algorithm [14,15] was used for data reconstruction. In the voxel-projection of the 3D reconstruction, shown in figure 5a, most of the dislocation helices and loops can be clearly observed, and the image fit well with the original 2D dislocation structure observations (figure 1b). By referring to the lattice orientation used during acquisition process, a 10° tilt about *z* axis was performed to adjust the reconstructed voxel close to the $[100]_{Al}$ direction, which allows the crystallographic orientations of the axes of helical dislocations to be readily determined. Combined with the Burgers vector analysis results (figure 2), the crystallography and morphology of the dislocation loops and helices could thus be fully characterized. All the visible dislocation loops were identified to be pure edge type full dislocations on {011} planes (marked by green arrows). For the three helical dislocations seen in this area, the 3D analysis revealed that their helical axes are parallel to [101], [01$\bar{1}$], and [10$\bar{1}$], respectively. No <001>-type axes of helical dislocations were observed. To be noted is that caution is needed in determining the axes of dislocation helices. For example, when viewing the dislocation helices from the [100] direction (figure 5a) both the helices of Burgers vectors [101] and [10$\bar{1}$] (marked yellow) appear to have their axes parallel to [001] direction. It is concluded that all the dislocation helices have their axes parallel to their Burgers vectors. These results are in good accordance with previous results [2,4,6,7].

The above results also indicate a possibility for a full 3D characterization of crystallography and morphology of dislocation structures by transforming the dislocation electron tomography in the sample coordinate system to the crystal coordinate system. More detailed analysis of the crystallographic features of dislocation structures are to be presented in a forthcoming paper.

4. Conclusions

The morphological and crystallographic features of dislocation loops and helices in a water-quenched Al-Cu-Mg alloy were characterized by means of dislocation tomography and Burgers vector analysis. The dislocation loops were identified to be pure edge type dislocations on {011} planes, while the axes of dislocation helices were determined to be parallel to their Burgers vectors, which were all of <110> type.

Acknowledgements

Financial supports from the National Natural Science Foundation of China (51501022, 51327805, 51471039), State Key Research and Development Program of MOST of China (2016YFB0700401), Natural Science Foundation of CQ (cstc2016jcyjA0266) and Fundamental Research Funds for the Central Universities (CDJZR14130002) are gratefully acknowledged.

References

[1] Totten G E and MacKenzie D S 2003 *Handbook of Aluminum: Physical Metallurgy and processes* vol I, ed Marcel Dekker (New York)
[2] Hull D and Bacon D J 2001 *Introduction to Dislocations* 4th ed Butterworth-Heinemann (Oxford)
[3] Embury J D and Nicholson R B 1963 *Acta Metall.* **11** 347
[4] Feng Z Q, Yang Y Q, Huang B, Luo X, Li M H, Han M and Fu M S 2011 *Acta Mater.* **59** 2412
[5] Wilson R N 1969 *J. Inst. Met.* **97** 80
[6] Thomas G and Whelan M J 1959 *Phil. Mag.* **40** 511
[7] Hutchinson C R and Ringer S P 2000 *Metall. Mater. Trans. A* **31A** 2721
[8] Raviprasad K, Hutchinson C R, Sakurai T and Ringer S P 2003 *Acta Mater.* **51** 5037
[9] Wilson R N, Moore D M and Forsyth P J E 1967 *J. Inst. Met.* **95** 177
[10] Barnard J S, Sharp J, Tong J R and Midgley P A 2006 *Science* **313** 319
[11] Tanaka M, Higashida K, Kaneko K, Hata S and Mitsuhara M 2008 *Scripta Mater.* **59** 901
[12] Liu G S, House S D, Kacher J, Tanaka M, Higashida K and Robertson I M 2014 *Mater. Charact.* **87** 1
[13] Amat F, Castano-Diez D, Lawrence A, Moussavi F, Winkler H and Horowitz M 2010 *Methods in Enzymology* **482** 343
[14] Jose-Jesus Fernandez 2012 *Micron* **43** 1010
[15] Jose-Jesus Fernandez 2012 *Current Opinion in Solid State and Materials Science* **17** 93